Acta Crystallographica Section B
Structural Science
ISSN 0108-7681

The modulated structure of the calcium aluminate $Ca_6(AlO_2)_{12}\cdot Bi_2O_3$

O. Pérez,* S. Malo and M. Hervieu

CRISMAT, UMR CNRS 6508, ENSICAEN, 6 Boulevard du Maréchal Juin, F-14050 Caen CEDEX 4, France

Correspondence e-mail: olivier.perez@ensicaen.fr

Received 5 May 2010
Accepted 6 September 2010

Bismuth calcium aluminate, $Bi_2Ca_6Al_{12}O_{27}$, has been prepared as a ceramic and a single crystal. Analysis of reciprocal space using both electron and X-ray diffraction show an *R*-centred hexagonal unit cell: $a = b = 17.3892\,(4)$, $c = 6.986\,(1)$ Å. Additional weak reflections are observed; they require the introduction of a modulation wavevector $\mathbf{q} = 0.0453\,(2)\mathbf{c}^*$ for indexing. The modulated structure has been solved using the superspace formalism [superspace group $X\bar{3}(00\gamma)0$]. A framework of corner-sharing AlO_4 tetrahedra forms corrugated sixfold rings and uncommon triple rings. The Ca^{2+} cations exhibit an eightfold coordination sphere; edge-sharing CaO_8 polyhedra form intertwinned zigzagging rows along **c** creating a three-dimensional net. Bi atoms are located in large hexagonal tunnels parallel to **c** and form Bi_2O_3 pairs, which adopt a trigonal bipyramidal configuration. The $6s^2$ lone-electron pairs (Lp) point along **c**, in the opposite direction to the three Bi—O strong bonds to form two BiO_3Lp tetrahedra with a common base. Different orientations of the $Bi_2O_3Lp_2$ pairs, rotated by 60° around **c**, are observed. Their stacking modes in each of the hexagonal tunnels are described. The sequence of the stacking varies along **c** in each of the tunnels.

1. Introduction

There has been considerable interest in the calcium-based aluminate compounds because of their actual and potential chemical and physical properties. For example, $Ca_3Al_2O_6$ ($3CaO\cdot 1Al_2O_3$ or C3*A*; Mondal & Jeffery, 1975) and $Ca_{12}Al_{14}O_{33}$ are important components of Portland and calcium aluminate cements. These materials have also attracted attention as ionic conductors, transparent conductors and catalysts thanks to their optical properties. These properties are indeed closely related to the alumina guest framework. $CaAl_2O_4$ (Vincent & Jeffery, 1978; Hörkner & Müller-Buschbaum, 1976) belongs to the stuffed tridymite derivatives AM_2O_4 (M = Si, Al, Fe, Ga, Li, Be, Mg, P ...), where the M cations are located in M_2O_7 units built from rings of six corner-sharing MO_4 tetrahedra, which manage cavities for the large A cations ($A = Na^+$, Ca^{2+}, Sr^{2+}, Ba^{2+}, Pb^{2+}...; Müller-Buschbaum, 2003). Considering the convention for the orientation of the apical O atoms of the tetrahedra, namely 'up' (U) and 'down' (D) with regard to the basal plane of the rings formed by six corner-sharing tetrahedra, the structure adopts an alternating arrangement UUDUDD + UDUDUD of the AlO_4 tetrahedra. $Ca_4Al_6O_{13}$ exhibits a sodalite-type structure, also observed for several aluminium-based ternary oxides with various compositions; they exhibit large cages

formed from tetrahedra, directly linked through six-membered rings and containing an anion (Pomarev *et al.*, 1970).

Bi-based oxides are also of interest for numerous applications, as in oxygen sensors or solid oxide fuel cells (Berastegui *et al.*, 1999), but only two phases have been structurally characterized in the pseudo-ternary Bi–*Ae*–Al–O system (where *Ae* represents alkaline earth, Sr^{2+} and/or Ca^{2+}), despite several other reports.

The first family, fullerenoid-type structures $(Sr_{1-x}Ca_x)_{33}Bi_{24}Al_{48}O_{141}$ ($0 \leq x \leq 1$), has similarities with the skeleton of sodalite owing to the existence of large spherical cages, and with the fullerene C84, *via* the AlO_4 tetrahedra arrangement (Hervieu *et al.*, 2004; Boudin *et al.*, 2005; Mellenne *et al.*, 2005; Retoux *et al.*, 2005). The Al84 spheres are filled with onion-like layers, made up of Sr and O species, surrounding a pseudo-spherical Bi cluster, $Bi_{16}O_{52}$, formed by six bipyramids Bi_2O_8 and four BiO_6 octahedra (Boudin *et al.*, 2005).

The second compound, $Sr_6(Al_{12}O_{24})\cdot Bi_2O_3$ (Bakakin *et al.*, 1994), exhibits a rhombohedral framework similar to that of the Bi-free phase $5SrO\cdot 4Al_2O_3\cdot H_2O$ or $Sr_{7.5}(Al_{12}O_{24})(OH)_3$ (Dent Glasser *et al.*, 1982). All the tetrahedra are corner sharing and form a framework which consists of corrugated sixfold rings and six triple rings (the structure will be further detailed). The main difference between the two structures is the presence of an original Bi_2O_3 group instead of Sr atoms.

At present, in the Bi–Ca–Al–O system, the only ternary oxide reported to our knowledge is the fullerenoid $Ca_{33}Bi_{22.7}Al_{48}O_{139.05}$ (Mellenne *et al.*, 2005). This paper presents the synthesis and the structural study of a second ternary oxide, $Bi_2Ca_6Al_{12}O_{27}$ or $Ca_6(AlO_2)_{12}\cdot Bi_2O_3$, which exhibits an incommensurate modulated structure.

2. Experimental

2.1. Synthesis

Different compositions and thermal processes were tested to prepare the powder samples starting from the oxides Bi_2O_3, CaO and Al_2O_3. X-ray powder diffraction (XRPD) data were collected at room temperature with an XPERT Pro Panalytical diffractometer with Co $K\alpha$ radiation (λ = 1.78901 Å) in the range $3 \leq 2\theta \leq 120^\circ$. The quality of the different samples was analysed from XRPD patterns. The best sample was prepared with a small excess of bismuth oxide, starting from Bi_2O_3, CaO and Al_2O_3 in the ratio 1.5/6/6. The mixture was introduced into a silica ampoule, heated at 1373 K for 48 h; the temperature was slowly decreased to 1273 K (2 K min^{-1}), to 873 K (4 K min^{-1}) and, lastly, to room temperature. Single crystals were grown, starting from the same precursors in the ratio 2.5/6/6. The ground mixture, introduced in a silica ampoule, was heated up to 1323 K in 24 h, maintained at this temperature for 48 h, decreased using a 2 K h^{-1} cooling rate down to 873 K and cooled down to room temperature.

2.2. Electron diffraction

Electron microscopy samples were prepared by crushing the crystallites in *n*-butanol; the small flakes in suspension were then deposited on a holey carbon film supported by a copper grid. Electron diffraction (ED) experiments were carried out using a Jeol 200CX electron microscope equipped with an EDS (X-ray energy-dispersive spectroscopy) analyzer.

The reconstruction of reciprocal space was carried out by tilting around the crystallographic axes. The electron-diffraction patterns (Fig. 1) are compatible with the following hexagonal cell: $a = b \simeq 17.5$ Å, $c \simeq 7$ Å and a primitive lattice. However, the observation of the [001] zone-axis pattern (ZAP; Fig. 1) reveals the existence of a set of intense reflections according to the conditions $hk\ell$: $-h + k + \ell = 3n$; reflections of a weaker intensity do not follow this condition. An accurate analysis of the [110] zone-axis pattern (Fig. 2*a*) shows the specific character of these weak reflections. They are slightly displaced along $\mathbf{c}^*$ so that they are not aligned on the row $[h00]^*$ (see Fig. 2*c*). As a result, the reflections breaking the condition $hk\ell$: $-h + k + \ell = 3n$ (observed in Fig. 1) are located in the highest reciprocal layer $(hk0 + \gamma)^*$. The [001] ZAP can be indexed using a hexagonal unit cell ($a = b \simeq 17.5$ Å and $c \simeq 7$ Å) with the *R* centring vector. The additional reflections of a weaker intensity are related to the existence of aperiodicities and must be considered as satellite reflections. Their indexing requires the introduction of the two symmetry-related modulation wavevectors $\mathbf{q} = \mathbf{a}^* + \gamma\mathbf{c}^*$ and $\mathbf{q}' = \mathbf{b}^* + \gamma\mathbf{c}^*$.

The irrational value of γ and the incommensurate modulation vector prevent a classical three-dimensional study of the structure. Consequently, a superspace approach is required to determine the accurate structure of $Ca_6(AlO_2)_{12}\cdot Bi_2O_3$ including the modulation effects.

The parameters of the subcell as well as the observation of the centring vector are consistent with those determined for the Sr-based aluminates (Bakakin *et al.*, 1994; Dent Glasser *et*

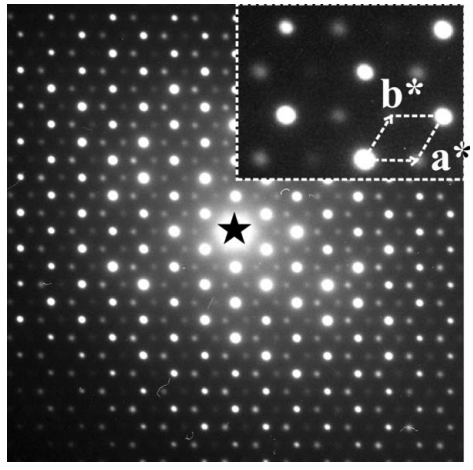

Figure 1
(*hk*0) electron-diffraction pattern. The trigonal subcell is drawn in the insert.

Table 1
Experimental details.

Crystal data	
Chemical formula	$Al_{12}Bi_2Ca_6O_{27}$
M_r	141.2
Crystal system, space group	Trigonal, $X\bar{3}(00\gamma)0$
Temperature (K)	293
Lattice centring	Rhombohedral
Wavevectors	$\mathbf{q} = 0.045\ (1)\mathbf{c}$
a, c (Å)	17.3892 (4), 6.986 (1)
V (Å^3)	1829.4 (3)
Z	3
F(000)	1974
Radiation type	Mo $K\alpha$
μ (mm^{-1})	17.21
Centring vector	$\frac{2}{3},\frac{1}{3},\frac{1}{3},\frac{2}{3}$ $\frac{1}{3},\frac{2}{3},\frac{2}{3},\frac{1}{3}$
Scan strategy	$\varphi-\omega$
Scan angle (°)	0.8
$(\sin\theta/\lambda)_{max}$	0.9
Crystal size (mm)	0.16 × 0.10 × 0.08 × 0.12 (radius)
Data collection	
Diffractometer	Nonius CCD
Absorption correction	Gaussian *JANA*2006
T_{min}, T_{max}	0.157, 0.290
No. of measured, independent and observed [$I > 3\sigma(I)$] reflections	22 743, 7371, 5668
Main reflections	2380
Satellites reflections, first-order	3288
R_{int}	0.039
Refinement	
$R[F^2 > 3\sigma(F^2)]$, $wR(F^2)$, S	0.043, 0.046, 2.82
No. of reflections	7371
No. of parameters	134
No. of restraints	0
$\Delta\rho_{max}$, $\Delta\rho_{min}$ (e Å^{-3})	5.13, −5.37
Reliability factors (R/wR)	0.040/0.045
Main reflections (R_0/wR_0)	0.0276/0.0378
Satellite reflections first-order (R_1/wR_1)	0.080/0.074

al., 1982). However, the existence of aperiodicities has never been reported for these Sr-based aluminates.

2.3. X-ray powder diffraction

The X-ray powder diffraction (XRPD) data were collected at room temperature with an X-PERT Pro Philips diffractometer with Co $K\alpha$ radiation (λ = 1.78901 Å) in the range $3 \leq 2\theta \leq 120°$. The XRPD diffractogram is compatible with the unit cell identified by electron diffraction (see §2.2). Additional peaks are also observed; they can be associated with the satellite reflections related to the modulated wavevectors **q** and **q**′. The cell parameters have been refined to a = 17.3415 (3) and c = 6.9695 (3) Å; the γ component of the wavevectors is refined to 0.046 (1). The diffraction pattern can be completely indexed as a single phase.

2.4. X-ray single-crystal diffraction

A preliminary single-crystal X-ray diffraction investigation was performed at room temperature using Mo $K\alpha$ radiation with a Kappa CCD (Bruker Nonius) diffractometer. Large φ and ω scans were used to monitor the crystalline quality of different crystals and to determine the cell parameters. A single crystal of suitable size (120 × 150 × 160 µm^3) was selected. Frames were then collected, for $0 < \theta < 40°$, with a classical strategy based on φ and ω scans, a small scan angle (0.8° per frame) and a short sample–detector distance (D_x = 34 mm; see Table 1).

The sections of reciprocal space calculated from this series of experimental frames are sufficiently accurate to obtain an overall view of reciprocal space. As previously explained in §2.2, two types of reflections can be seen [see for example the (h0ℓ) plane in Fig. 2*c*]. The intense spots are characteristic of a hexagonal sub-cell [$a = b$ = 17.3892 (4), c = 6.986 (1) Å], while the weaker ones are in incommensurate positions; the two symmetry-related $\mathbf{q} = \mathbf{a}^* + \gamma\mathbf{c}^*$ and $\mathbf{q}' = \mathbf{b}^* + \gamma\mathbf{c}^*$ vectors must be introduced to index them. The γ component of the modulation vector has been refined to γ = 0.0453 (2) for the crystal studied. An accurate analysis then requires the superspace formalism to be developed for incommensurate modulated structures.

Following the observed conditions for diffraction the whole pattern can also be described using the basic hexagonal subcell and introducing both the modulation vector $q = \gamma\mathbf{c}^*$ and the X centring in the (3 + 1)-dimensional space: ($\frac{2}{3},\frac{1}{3},\frac{1}{3},\frac{2}{3}$; $\frac{1}{3},\frac{2}{3},\frac{2}{3},\frac{1}{3}$).

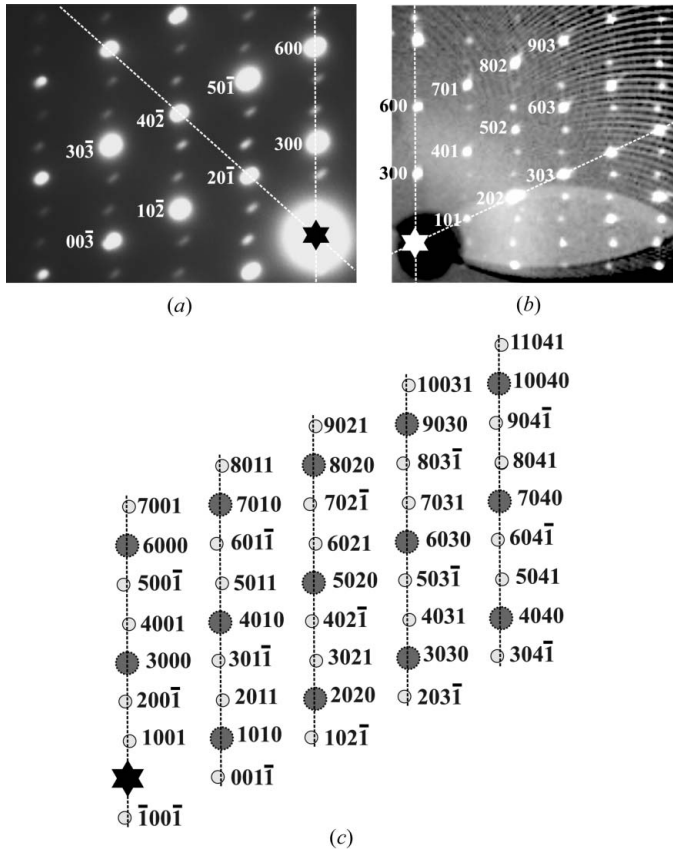

Figure 2
(h0ℓ) diffraction pattern. (*a*) Electron diffraction and (*b*) X-ray diffraction. The misalignment of the satellite reflections with the vertical line (*i.e.* the existence of the small component for the modulation vector along **c**) is shown. The indexing given in (*c*) was done with the four integers $hk\ell m$, m refering to $\mathbf{q} = 0.045\mathbf{c}^*$ (m = 0 for main reflections and $m \neq 0$ for satellites).

EvalCCD software (Duisenberg *et al.*, 2003) was used to extract reflections from the collected frames. The internal R values, calculated for the $\bar{3}$, $\bar{3}1m$, $\bar{3}m1$ Laue classes (equal to 0.0577, 0.1928 and 0.4134) clearly allow us to determine unambiguously the class as $\bar{3}$. The superspace groups compatible with these observations are then $X\bar{3}(00\gamma)0$ and $X3(00\gamma)0$.

Data were corrected for absorption using the *JANA*2006 program (Petříček *et al.*, 2006) within the analytical option based on crystal morphology; *X-SHAPE* software (Stoe & Cie, 1998) was used to optimize the morphology. Details of the data collection are summarized in Table 1.

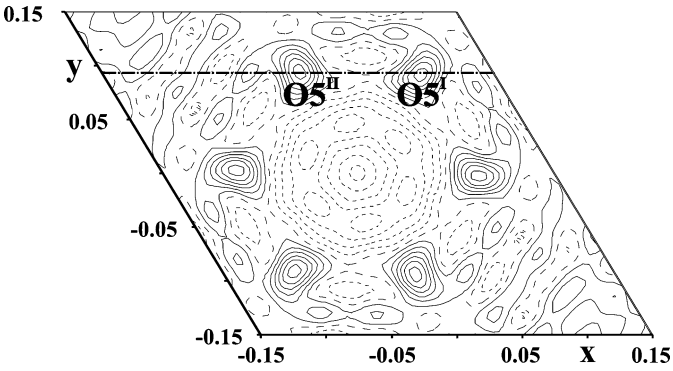

Figure 3
Difference-Fourier map calculated around the position expected for O5; a summation from $x_3 = -0.015$ to 0.015 is applied. Six oxygen sites are clearly visible. $O5^{i}$ and $O5^{ii}$ are too close to coexist: they can be interpreted as disordered oxygen sites.

2.5. Structure determination

2.5.1. The average structure. A starting model was defined from the structure published for $Sr_6(Al_{12}O_{24})\cdot Bi_2O_3$ (Bakakin *et al.*, 1994). The average structure is described by nine crystallographically independant atoms: one Ca atom, two Al atoms Al1 and Al2, five O atoms O1, O2, O3, O4 and O5 (located on the 18*f* sites), and one Bi atom located on the 6*c* site. The six equivalent O5 atoms generated by the threefold axis and the inversion centre surround the Bi atoms (see Fig. 3); their occupancy is equal to $\frac{1}{2}$. Moreover, the atomic distances between two O5 sites, equivalent by a $\bar{3}$ axis, are too short (≤ 1.7 Å) and prevent the coexistence of the six O5 atoms. The final refinement converged to an agreement factor $R_F = 0.0306$ for the 2380 main reflections [with $I \geq 3\sigma(I)$]. Note that the observation of short O—O distances and the occupancy factor of O5 which refined to $\frac{1}{2}$ are in agreement with the result already published by Bakakin *et al.* (1994).

2.5.2. HREM analysis. The high-resolution electron-microscopy study was performed with a FEI TECNAI 30 G^2 electron microscope, working at 300 KV (Cs = 0.7 mm). This microscope was equipped with a KEVEX EDS analyzer. Theoretical images were calculated using the *MacTempas* program (O'Keefer & Kilaas, 1987) with the atomic positions deduced from the single-crystal X-ray diffraction study (see §2.5.1). Two typical contrasts of the [001] high-resolution electron microscopy images, recorded in the course of the through focus series, are given in Fig. 4 (the calculated images for a crystal thickness of 42 Å are given as inserts in both figures). In Fig. 4(*a*) the high electron-density zones appear as the darker dots (focus value close to −300 Å). The characteristic contrast consists of a regular array of dark dots surrounded by a white sixfold star: the centre of the star is associated with the Bi positions located in the tunnels and the white star to the zone of low electron density in between the dark dots of Bi and the six Ca (and Al) positions (see the schematic representation at the top of Fig. 4*a*). In Fig. 4(*b*) these positions appear as the brighter zones (focus close to −1200 Å); the brighter zones are correlated with the Bi positions, surrounded by six Ca (and Al) positions and separated from the adjacent Bi positions by two Ca

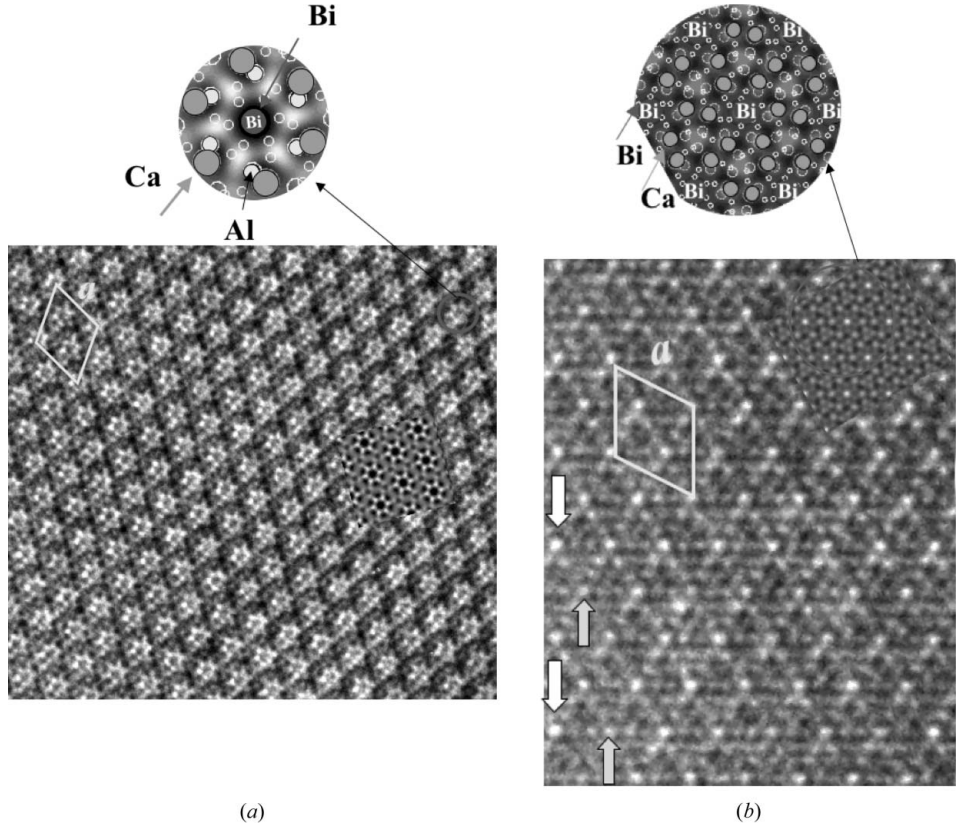

Figure 4
[001] HREM images with the calculated ones superimposed. The cation positions are imaged as (*a*) dark spots and (*b*) bright spots.

(and Al) positions (see schematical representation above the image). These experimental images show good agreement with those calculated.

No extended defects have been observed in this $Bi_2Ca_6Al_{12}O_{27}$ aluminate, attesting to its high degree of crystallinity. Only local variations of contrast, in the thin parts of the crystals, have been detected at the level of the Bi positions. This is illustrated, for example, in Fig. 4(*b*) by the vertical white arrows highlighting the contrast between two adjacent Bi dots. This localized contrast variation suggests a surface effect with a tiny loss of Bi and could be related to the small Bi deficiency (roughly 5%) observed by EDS analyses for some crystallites.

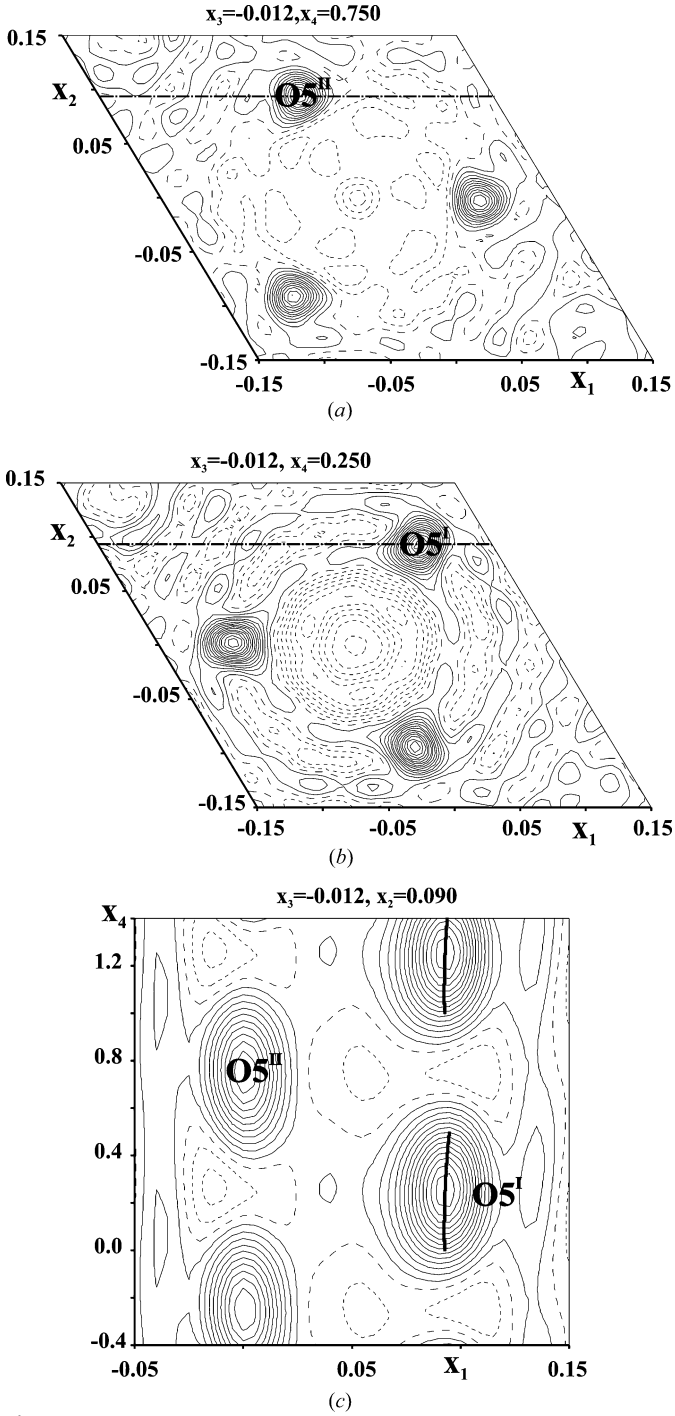

Figure 5
Four-dimensional Fourier map calculated around the position expected for O5 atoms. (*a*) and (*b*) $x_1 - x_2$ sections calculated for $x_4 = \frac{3}{4}$ and $\frac{1}{4}$. A summation from $x_3 = -0.015$ to 0.015 is applied. (*c*) $x_1 - x_4$ section showing two discontinuous atomic domains centred on $x_1 \simeq 0$ and 0.09. $O5^{i}$ and $O5^{ii}$ correspond to the two disordered oxygen sites reported in Fig. 3.

Table 2
Structural parameters.

r_0, s,1 and c,1 correspond to the average parameters, sine and cosine first-order Fourier terms.

		x	*y*	*z*	U_{iso} (Å^2)
Bi1	r_0	0.6667	0.3333	0.12054 (2)	0.01380 (9)
	s,1	0	0	0.00801 (7)	
	c,1	0	0	−0.01145 (6)	
Ca1	r_0	0.10863 (3)	0.85820 (3)	0.09300 (6)	0.00961 (12)
	s,1	−0.00544 (4)	−0.00566 (4)	0.00314 (7)	
	c,1	0.00346 (4)	0.00382 (4)	0.00021 (7)	
Al1	r_0	0.20779 (4)	0.74190 (4)	0.12907 (9)	0.00517 (17)
	s,1	−0.00320 (6)	−0.00284 (6)	−0.00256 (11)	
	c,1	0.00058 (6)	0.00208 (6)	−0.00607 (11)	
Al2	r_0	0.04922 (4)	0.64324 (4)	0.39891 (9)	0.00491 (18)
	s,1	−0.00041 (6)	−0.00450 (6)	0.00124 (11)	
	c,1	0.00542 (6)	0.00402 (6)	0.00091 (10)	
O1	r_0	0.12453 (10)	0.73893 (10)	0.2747 (2)	0.0082 (4)
	s,1	−0.00238 (15)	−0.00348 (14)	0.0016 (3)	
	c,1	0.00467 (15)	0.00473 (14)	0.0029 (3)	
O2	r_0	0.22615 (11)	0.81541 (10)	−0.0573 (2)	0.0094 (4)
	s,1	−0.00435 (15)	−0.00115 (14)	0.0028 (3)	
	c,1	−0.00005 (15)	0.00499 (14)	0.0003 (3)	
O3	r_0	0.18035 (12)	0.63527 (11)	0.0496 (2)	0.0112 (5)
	s,1	−0.00302 (16)	−0.00249 (15)	−0.0059 (3)	
	c,1	−0.00403 (17)	0.00117 (15)	−0.0102 (3)	
O4	r_0	−0.05846 (10)	0.59734 (11)	0.3071 (2)	0.0072 (4)
	s,1	−0.00055 (14)	−0.00560 (14)	0.0012 (2)	
	c,1	0.00619 (14)	0.00374 (15)	−0.0022 (2)	
O5	r_0	0.0935 (3)	0.0919 (3)	−0.0124 (5)	0.0147 (8)
	S_1^O†	0.0011 (4)	−0.0014 (4)	−0.0002 (7)	
	S_1^E†	0.0008 (16)	0.0013 (17)	0.003 (3)	
Crenel function					
	Δ‡	0.5			
	$\bar{x}_4^0$	0.24944			

† Odd (S_O) and even (S_E) terms of the Legendre polynomials. ‡ Fixed during the refinement.

2.5.3. The modulated structure. The modulated structure of $Ca_6(Al_{12}O_{24})\cdot Bi_2O_3$ was solved using the superspace formalism (de Wolff *et al.*, 1981) developed for the study of incommensurate phases. The introduction of an additional dimension defined by a vector orthogonal to real space allows the recovery of a periodicity. In this description (see Janssen *et al.*, 2010, for a general description of the superspace formalism), each atom is characterized by an average position and/or occupancy (or anisotropic displacement parameter, ADP) and a deviation from these average parameters in the additional direction. Usually knowledge of the average structure provides some information on determining a preliminary model for the modulation. In the present case the average structure reveals both an apparent disorder observed for the O5 atoms and an ADP along **c** for Bi more than two times larger than that along **a** or **b**. These two features suggest that the modulation in the structure mainly affects Bi and O5 atoms. Owing to the difference between the atomic scattering

factors of Bi and O, a preliminary model for the modulation was built giving a reasonable isotropic ADP (0.01 Å^2) to Bi and an atomic displacement along **c** (expanded as a Fourier series up to first order). The amplitude of the displacement was estimated from the U^{33} value refined for the average structure; the sign of the displacement was chosen *via* trial and error using only the satellite reflections; the Fourier terms were mainly sensitive to the satellites. An agreement factor of $R_F = 0.41$ was obtained on these reflections. Just by refining average and modulated parameters for Bi using all the reflections, the reliability factor reached the value of $R_F = 0.30$. Observed Fourier maps can then be calculated around the position expected for O5. The $x_1 - x_2$ sections calculated for $x_4 = \frac{1}{4}$ and $x_4 = \frac{3}{4}$ (see Figs. 5*a* and *b*) show dramatic modifications of the electron density corresponding to the O5 atoms in comparison with those observed for the average structure (see Fig. 3). The O5^{i} and O5^{ii} sites (O5^{i} and O5^{ii} are in the superspace approach made equivalent by the inversion axis $\overline{3}$: $x_1 - x_2, x_1, \overline{x}_3, \overline{x}_4$) previously identified in Fig. 3 are no longer present for the same x_4 domain (see Fig. 5*c*). It results in a near-perfect ordering of the O5 atoms in the modulated structure. A crenel function was then introduced to describe the O5 atom. The full separation of crenels for O5^{i} and O5^{ii} is realised only if the equation

$$t^0[\mathrm{O5^{ii}}] = t^0[\mathrm{O5^{i}}] + \frac{1}{2} \Rightarrow x_4^0[\mathrm{O5^{i}}] = \gamma z[\mathrm{O5^{i}}] + \frac{1}{4} \qquad (1)$$

is fulfilled. This equation is introduced in the refinement; owing to the small value of γ, x_4^0[O5^{i}] is close to $\frac{1}{4}$. Displacements of this atom were defined using Legendre polynomials (see Roussel *et al.*, 2010, for the expression of the atomic position vector); these polynomials are orthogonal by definition and therefore the orthogonalization procedure can be neglected (Petříček *et al.*, 1995).

Atomic displacements were considered (expanded as Fourier series up to first order) and refined for all the other atoms (Ca, Al1, Al2, O1, O2, O3 and O4). Finally, a modulation of the ADP was introduced up to second order for the Bi site (although no second-order satellite reflections are observed, second-order terms lead to an improvement of the reliability factor), which takes into account the modification of the environment of the atoms because of O5 ordering and displacive modulation affecting Bi. Refinement parameters are summarized in Table 2; anisotropic and modulated ADPs are given in the supplementary information.[1] The final reliablity factors are R_F = 0.0276 and 0.0800 for the main and satellite reflections.

3. Structural description

3.1. The $Ca_6Al_{12}O_{24}$ framework

Amplitudes of the modulations affecting Al1, Al2, O1, O2, O3 and O4 are small and consequently the $Al_{12}O_{24}$ tetrahedral skeleton (Fig. 6) is close to that previously described by Bakakin *et al.* (1994). Al1 and Al2 sites exhibit four Al—O distances ranging between 1.738 and 1.785 Å. They are characteristic of the tetrahedral coordination of Al and can be directly compared with those observed in the alumina structures (Zhou & Snyder, 1991; Husson & Repelin, 1996). Each AlO_4 tetrahedron shares all of its corners with four other tetrahedra. This feature leads to the formation of unusual Al_3O_9 rings (see Fig. 6), with three O—O interatomic distances close to 2.9 Å and O—O—O angles close to 60°. Such a threefold ring has been encountered as Si_3O_9 rings in silicates of the related wollastonite $CaSiO_3$ (Yang & Prewitt, 1999; Joswig *et al.*, 2003) and Ge_3O_9 rings in $PbGe_4O_9$ (Bush & Stephanovitch, 2002) and $Sb_2Ge_3O_9$ (Ke *et al.*, 2002). In the latter the Ge_3O_9 rings are connected by pairs to trigonal pyramids SbO_3. The only other family exhibiting the Al_3O_9 rings is that of the Sr- and Ca-based fullerenoids (Hervieu *et al.*, 2004; Boudin *et al.*, 2005; Mellenne *et al.*, 2005; Retoux *et al.*, 2005). The connection of three Al_3O_9 units manages sixfold rings Al_6O_{18} (Fig. 6), which are arranged in a 'UUUDDD' mode, using the nomenclature of the stuffed tridymite-related compounds. Similar sequences have been reported in γ-$SrGa_2O_4$ (Kahlenberg *et al.*, 2000) and in one recent structure of $SrFe_2O_4$ (Kahlenberg & Fischer, 2001). Bi1 and O5 atoms are inserted within the so-built hexagonal tunnels, while a Ca atom occupies one part of the as-managed cages (Fig. 6). The calculated average distortion indices D_{ind} ($D_{\mathrm{ind}} = \frac{1}{6}\sum_{i=1}^{i=6}(\theta_i - 109°7)^2$) are 12.9 for the $Al1O_4$ (tetrahedra defining the hexagonal tunnel contour) and 41.1 for the $Al2O_4$ tetrahedra, indicating a high distortion which could be correlated to the distribution of the Bi and O5 atoms in the hexagonal tunnels along **c**.

The determination of the modulated structure has revealed a 'disorder' preventing the accurate location of the O5 atoms in an average description. Consequently, since this oxygen belongs to the first calcium neighbour, the modulation reveals the true nature of the calcium environment. Ca atoms exhibit

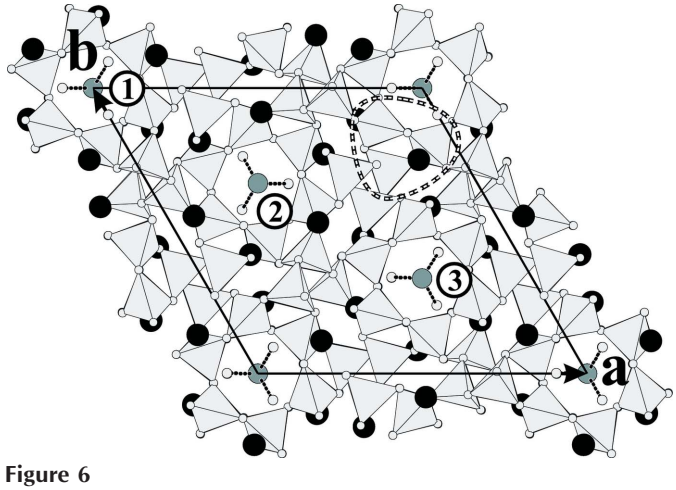

Figure 6
Projection along **c** of the structure of $Ca_6(AlO_2)_{12}{\cdot}Bi_2O_3$: the representation is based on the AlO_4 tetrahedra. The Ca, Bi and O atoms were drawn using black, grey and white disks. A dashed line surrounds the uncommon Al_3O_9 rings.

[1] Supplementary data for this paper are available from the IUCr electronic archives (Reference: SN5097). Services for accessing these data are described at the back of the journal.

an eightfold coordination sphere, with Ca—O distances ranging between 2.33 and 2.78 Å. Fig. 7(*a*) shows a representation of the structure based on CaO_8 polyhedra. The three-dimensional polyhedral net can be described from infinite zigzagging rows (white or grey polyhedra drawn in Fig. 7*b*) formed by edge-sharing of the CaO_8 polyhedra along **c**. Each polyhedron of a row shares one edge (and only one) with another polyhedron belonging to an adjacent row. Ribbons four rows wide outlined by a dotted line are shown in Fig. 7(*a*); triangular tunnels are generated by a 120° rotation of this object around the vertical axis located at $\frac{2}{3}\mathbf{a}, \frac{1}{3}\mathbf{b}$; they host Bi1 and O5 atoms.

3.2. Filling of the hexagonal tunnels with Bi_2O_n groups

Two types of Bi—Bi interatomic distances, ranging from 2.969 (1) to 2.977 (1) Å and from 3.982 (1) to 4.044 (1) Å, alternate along **c**, forming bismuth pairs (or 'dimers'). Looking at the O5 modulation mechanism, three O5 atoms assuming Bi—O distances ranging from 2.15 (2) to 2.25 (2) Å are located in the equatorial plane of each dimer. Note that the three Bi—O5 interatomic distances are of the same order as those observed in the α form of Bi_2O_3 (Harwig, 1978). The resulting Bi_2O_3 entities are surrounded by six O3 atoms with 2.697 (4) Å $\leq d_{Bi-O3} \leq$ 2.719 (4) Å. Bond-valence calculations, following the approach developed by Brown (1996), are in agreement with Bi^{3+} species well known for exhibiting a $6s^2$ lone pair (Lp). Lone-pair positioning was widely discussed by Jakubowicz *et al.* (1998): the Bi^{3+} cation adopts different coordinations in BiO_x polyhedra, but is systematically characterized by a strong stereoactivity of the lone-electron pair. The location of the electronic lone pair for each of the Bi atoms has been obtained using electrostatic equilibrium models for complex oxides such as $Bi_{2+x}Sr_{3-x}Fe_2O_{9+\delta}$ (Pérez *et al.*, 1995; Pérez, Leligny, Grebille *et al.*, 1997), $[Bi_{0.87}SrO_2]_2[CoO_2]_{1.82}$ (Leligny *et al.*, 2000), $Bi_{6+x}Sr_{9-x}Fe_5O_{26}$ and $Bi_{14}Sr_{21}Fe_{12}O_{61}$ (Pérez, Leligny, Baldinozzi *et al.*, 1997; Hervieu *et al.*, 1997; Allix *et al.*, 2004). Owing to aperiodicity phenomena or shearing mechanisms, these compounds provide a great number of different $Bi^{3+}O_nLp$ environments. All cases between the extreme limits of an ideal tetrahedron and of a distorted bipyramid are encountered for the Bi environment, but the lone pair is always located in the opposite direction to the three shorter Bi—O distances. The case of an ideal BiO_3Lp tetrahedron, already observed for $Bi_4Sr_{12}Co_8O_{30-\delta}$ (Perez *et al.*, 2002) with the electronic lone pair of Bi^{3+} perpendicular to the plane defined by the three O atoms, seems to be the most appropriate to describe the bismuth environment in $Ca_6(Al_{12}O_{24})\cdot Bi_2O_3$. The $6s^2$ lone-electron pairs (Lps) point along **c**, in the opposite direction to the three Bi—O5 strong bonds, forming BiO_3Lp tetrahedra with a (3 + 1) coordination of bismuth. The full coordination sphere around Bi^{3+} accounting for the weaker Bi—O3 interactions leads to $Bi_2O_9Lp_2$ bismuth oxide cluster (drawn in Fig. 8*a*).

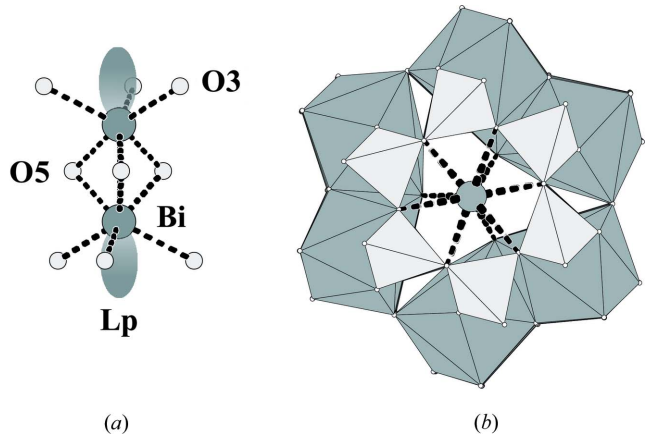

(*a*) (*b*)

Figure 8
(*a*) The $Bi_2O_9Lp_2$ clusters; Lp are symbolized by grey ellipsoids. (*b*) Projection of one hexagonal tunnel along **c**. AlO_4 and CaO_8 polyhedra are drawn in white and grey, respectively.

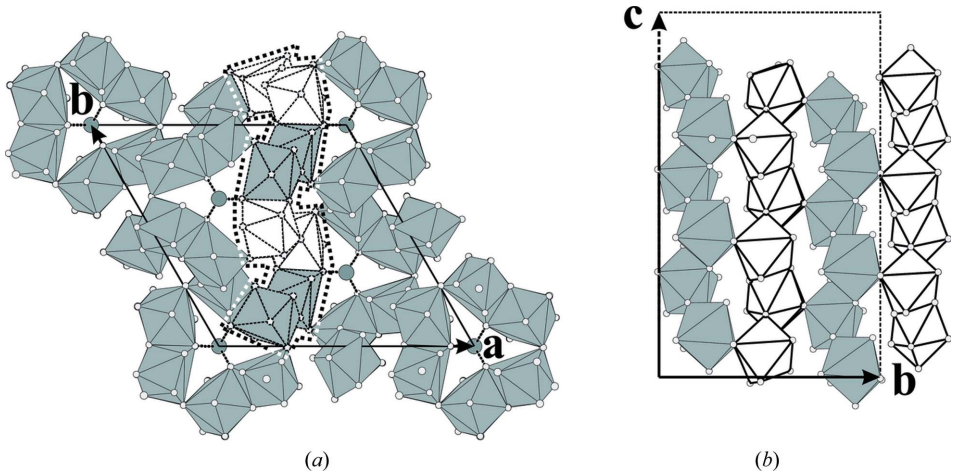

(*a*) (*b*)

Figure 7
Representation of the structure of $Ca_6(AlO_2)_{12}\cdot Bi_2O_3$ *via* the calcium framework. (*a*) Projection along **c**: triangular tunnels with Bi atoms as guest atoms and $[Ca_4O_{20}]_\infty$ ribbon (one of them is highlighted by a dashed line). (*b*) Projection along **a** of one $[Ca_4O_{20}]_\infty$ ribbon running along **c**; it is built from files (drawn in white or grey colour) of corner-sharing CaO_8 polyhedra connected *via* edges.

As shown in Fig. 6 the $Bi_2O_9Lp_2$ clusters are inserted in the large hexagonal tunnels. Analyses of the framework based on the AlO_4 and CaO_8 polyhedra previously performed in §3.1 must be combined to obtain the structure of these tunnels (see Fig. 8*b*); they indeed result in the regular stacking of Al_6O_{18} and Ca_6O_{39} rings (see Fig. 9*a*). Fig. 9*b* shows a view of the tunnel perpendicular to **c** without the Ca_6O_{39} rings; this illustrates the connections of the bismuth oxide clusters within the hexagonal tunnels. The O5 atoms only belong to coordination spheres of Ca and Bi atoms. Owing to the incommensurate character of the

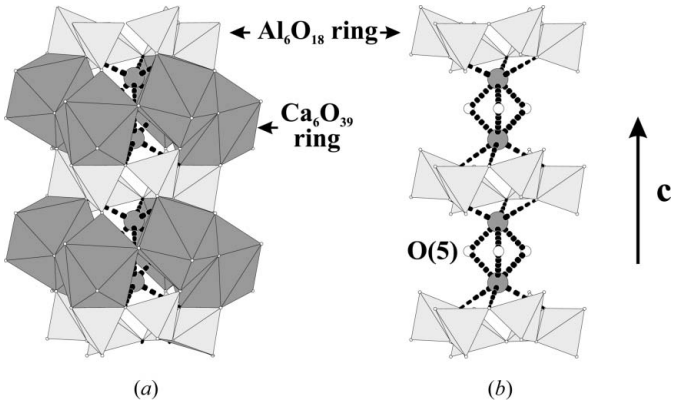

Figure 9
[110] projection of one hexagonal tunnel (*a*) with and (*b*) without the CaO_8 polyhedra. The Bi_2O_9 clusters are drawn within the tunnel.

modulation and the peculiar nature of the $X(\frac{2}{3}, \frac{1}{3}, \frac{1}{3}, \frac{2}{3}, \frac{1}{3}, \frac{2}{3}, \frac{2}{3}, \frac{1}{3})$ centring, the contents of the tunnels labelled 1, 2 and 3 (see Fig. 6) are no longer equivalent in physical three-dimensional space so must be analysed at the same time. Fig. 10 provides a schematic view of the filling of these three tunnels. For each tunnel, sequences which are built from approximately 11 clusters exhibiting the same orientation alternate along **c**; each sequence is rotated by 60° to that of the following sequence.

4. Conclusion

Comparison between $Sr_6(Al_{12}O_{24})\cdot Bi_2O_3$ (Bakakin *et al.*, 1994) and the present structure of $Bi_2Ca_6Al_{12}O_{27}$ shows a decrease in the cell volume (from 2229.4 to 2112.4 Å^3), Δ, of the order of 5%, smaller than expected considering the cation radii in VIII coordination ($\simeq$ 11%). In the same way, compared with $5SrO\cdot 4Al_2O_3\cdot H_2O$ (Dent Glasser *et al.*, 1982), the replacement of the cations located in the hexagonal tunnels does not significantly modify the cell volume ($\Delta V \simeq 3\%$). This shows that the architecture of the tetrahedral host, $[Al_{12}O_{24}]_{\infty}^{12-}$, which is the common framework of the three average structures, easily accommodates the different species and is sufficiently flexible to adapt to the interactions with the possible guests at their interface in the hexagonal tunnels of the structure.

In the structure of $Bi_2Ca_6Al_{12}O_{27}$ the cages or tunnels formed by the alumina framework define several favourable atomic sites which cannot be simultaneously occupied because of the small distances between them. The existence of these extra sites leads to a degree of freedom in the structure favourable for disorder or aperiodicities, as already reported for numerous tunnel compounds (Boullay *et al.*, 1997; Hervieu *et al.*, 1997; Baldinozzi *et al.*, 1996; Gillie *et al.*, 2005; Leligny *et al.*, 1993). Moreover, frameworks accommodating lone-pair cations (see Raveau *et al.*, 1991, for the Bi-based superconducting cuprates; Pérez *et al.*, 1995; Pérez, Leligny, Baldinozzi *et al.*, 1997; for Bi-based ferrites; Leligny *et al.*, 1999; for Bi-based cobaltites) commonly exhibit aperiodicities. The coexistence of several favourable atomic sites and Bi^{3+} species in $Ca_6(Al_{12}O_{24})\cdot Bi_2O_3$ is in agreement with the observation of aperiodicities. Analysis of the modulated structure, using the superspace formalism, provides an accurate description of $Ca_6(Al_{12}O_{24})\cdot Bi_2O_3$ showing near-perfect ordering of $Bi_2O_9Lp_2$ clusters in the hexagonal tunnels defined by the $Ca_6(Al_{12}O_{24})$ framework. The $Bi_2O_9Lp_2$ clusters exhibit different orientations along the tunnel axis (rotation of 60° from one to another), but the stacking of the different orientations in the tunnels is almost perfectly defined. Similar ordering of the $Bi_2O_9Lp_2$ clusters can be expected for $Sr_6(Al_{12}O_{24})\cdot Bi_2O_3$. The structure solution of Bakakin *et al.* (1994) reveals fractional occupancy factors for oxygen sites as

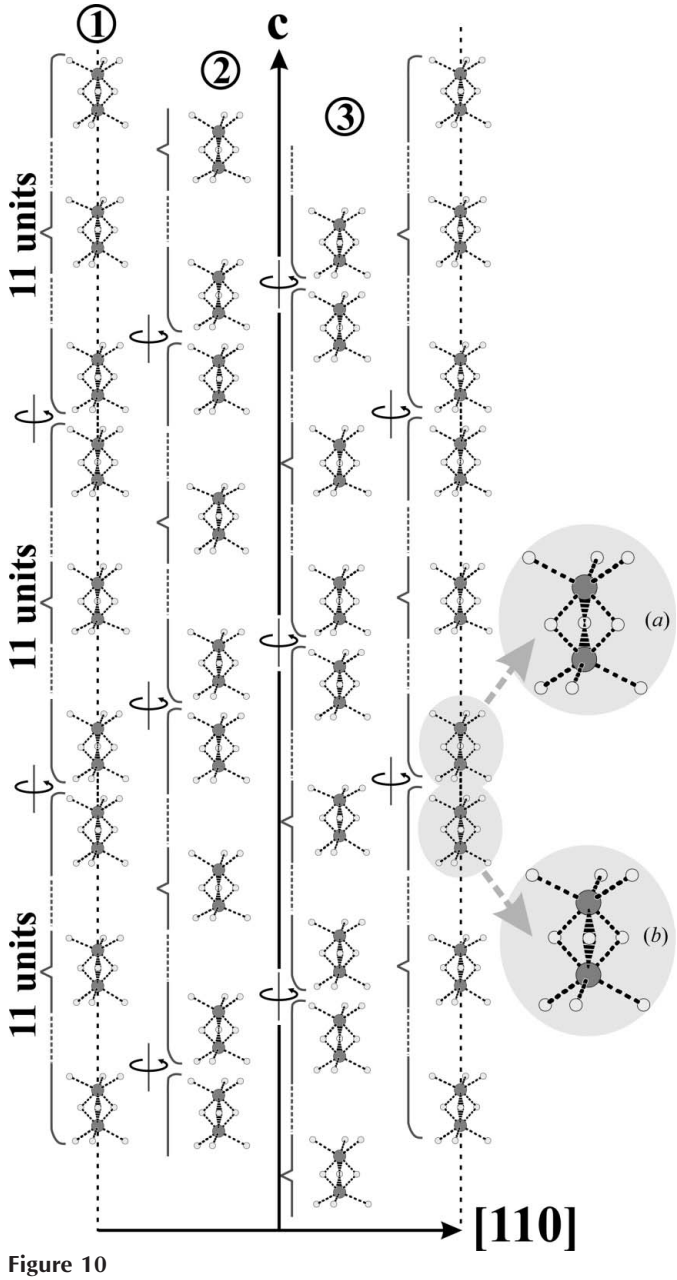

Figure 10
Schematic view of the filling of the three tunnels labelled 1, 2 and 3 in Fig. 6. For each tunnel the sequences of Bi_2O_9 clusters are reported. For each change in orientation (a rotation of 60° around **c**) of the clusters in the tunnels a circular arrow is drawn. Braces identified sequences of clusters with the same orientation. (*a*) and (*b*) provide the magnification of two orientations for Bi_2O_9.

reported for the average structure of $Ca_6(Al_{12}O_{24})\cdot Bi_2O_3$. Although not shown, an almost perfectly defined distribution of the $Bi_2O_9Lp_2$ clusters cannot be rejected: the use of point detector and classical X-ray sources during the data collection of Bakakin *et al.* (1994) should prevent the observation of satellite reflections.

References

Allix, M., Ṕerez, O., Pelloquin, D., Hervieu, M. & Raveau, B. (2004). *J. Solid State Chem.* **177**, 3187–3196.

Bakakin, V., Podberezkaya, N., Mazus, M., Kozeeva, L., Shaburova, V. & Malinovskii, T. (1994). *J. Struct. Chem.* **35**, 229–235.

Baldinozzi, G., Goutenoire, F., Hervieu, M., Suard, E. & Grebille, D. (1996). *Acta Cryst.* B**52**, 780–789.

Berastegui, P., Eriksson, S. & Hull, S. (1999). *Mater. Res. Bull.* **34**, 303–314.

Boudin, S., Mellenne, B., Retoux, R., Hervieu, M. & Raveau, B. (2005). *Inorg. Chem.* **43**, 5954–5960.

Boullay, P., Hervieu, M. & Raveau, B. (1997). *J. Solid State Chem.* **132**, 239–246.

Brown, I. D. (1996). *J. Appl. Cryst.* **29**, 479–480.

Bush, A. & Stephanovitch, S. (2002). *Inorg. Mater.* **38**, 168–171.

Dent Glasser, L. S., Henderson, A. P. & Howie, R. A. (1982). *Acta Cryst.* B**38**, 24–27.

Duisenberg, A. J. M., Kroon-Batenburg, L. M. J. & Schreurs, A. M. M. (2003). *J. Appl. Cryst.* **36**, 220–229.

Gillie, L., Hadermann, J., Pérez, O., Martin, C. & Hervieu, M. & Suard, E. (2005). *J. Solid State Chem.* **177**, 3383–3391.

Harwig, H. (1978). *Z. Anorg. Allg. Chem.* **444**, 151–166.

Hervieu, M., Mellenne, B., Retoux, R., Boudin, S. & Raveau, B. (2004). *Nature Mater.* **3**, 269–273.

Hervieu, M., Ṕerez, O., Groult, D., Grebille, D., Leligny, H. & Raveau, B. (1997). *J. Solid State Chem.* **129**, 214–222.

Hörkner, W. & Müller-Buschbaum, H. (1976). *J. Inorg. Nucl. Chem.* **38**, 983–984.

Husson, E. & Repelin, Y. (1996). *Eur. J. Solid State Inorg. Chem.* **33**, 1223–1231.

Jakubowicz, N., Pérez, O., Grebille, D. & Leligny, H. (1998). *J. Solid State Chem.* **139**, 194–199.

Janssen, T., Chapuis, G. & de Boissieu, M. (2010). IUCr Monographs on Crystallography, Vol. 20. Oxford Science Publication.

Joswig, W., Paulus, E., Winkler, B. & Milman, V. (2003). *Z. Kristallogr.* **218**, 811–818.

Kahlenberg, V. & Fischer, R. (2001). *Solid State Sci.* **3**, 433–439.

Kahlenberg, V., Fischer, R. & Shaw, C. (2000). *J. Solid State Chem.* **153**, 294–300.

Ke, Y., Li, J., Zhang, Y., Lu, S. & Lei, Z. (2002). *Solid State Sci.* **4**, 803–806.

Leligny, H., Grebille, D., Pérez, O., Masset, A., Hervieu, M., Michel, C. & Raveau, B. (1999). *C. R. Acad. Sci. C. Chim.* **2**, 409–414.

Leligny, H., Grebille, D., Pérez, O., Masset, A. C., Hervieu, M. & Raveau, B. (2000). *Acta Cryst.* B**56**, 173–182.

Leligny, H., Labbe, P., Ledesert, M., Hervieu, M., Raveau, B. & McCarroll, W. H. (1993). *Acta Cryst.* B**49**, 444–454.

Mellenne, B., Boudin, S., Retoux, R., Hervieu, M. & Raveau, B. (2005). *Mater. Res. Bull.* **40**, 1388–1401.

Mondal, P. & Jeffery, J. W. (1975). *Acta Cryst.* B**31**, 689–697.

Müller-Buschbaum, H. (2003). *J. Alloys Compd.* **349**, 49–104.

O'Keefer, M. & Kilaas, R. (1987). *macTempas Software Package*, XIIIth Western Regional Meeting for Electron Microscopy and Microbeam Analysis, Concord, California.

Pérez, O., Leligny, H., Baldinozzi, G., Grebille, D., Hervieu, M., Labbé, P., Groult, D. & Graafsma, H. (1997). *Phys. Rev. B*, **56**, 5662–5672.

Pérez, O., Leligny, H., Grebille, D., Grenêche, J., Labbé, P., Groult, D. & Raveau, B. (1997). *Phys. Rev. B*, **55**, 1236–1246.

Pérez, O., Leligny, H., Grebille, D., Labbé, P., Groult, D. & Raveau, B. (1995). *J. Phys. Condens. Matter*, **7**, 10003–10014.

Perez, O., Masset, A. C., Leligny, H., Baldinozzi, G., Pelloquin, D. & Dutheil, M. (2002). *Acta Cryst.* B**58**, 191–197.

Petříček, V., Dušek, M. & Palatinus, L. (2006). *JANA*2006. Institute of Physics, Praha, Czech Republic.

Petříček, V., van der Lee, A. & Evain, M. (1995). *Acta Cryst.* A**51**, 529–535.

Pomarev, V., Keiker, D. & Belov, N. (1970). *Kristallografiya*, **15**, 918–921.

Raveau, B., Michel, C., Hervieu, M. & Groult, D. (1991). *Springer Series in Materials Science*, 15th ed. Berlin, New York: Springer-Verlag.

Retoux, R., Mellenne, B., Boudin, S., Hervieu, M. & Raveau, B. (2005). *Solid State Sci.* **7**, 736–744.

Roussel, P., Pérez, O., Quarez, E., Leligny, H. & Mentré, O. (2010). *Z. Kristallogr.* **225**, 1–11.

Stoe & Cie (1998). *X-SHAPE.* Darmstadt, Germany.

Vincent, M. G. & Jeffery, J. W. (1978). *Acta Cryst.* B**34**, 1422–1428.

Wolff, P. M. de, Janssen, T. & Janner, A. (1981). *Acta Cryst.* A**37**, 625–636.

Yang, H. & Prewitt, C. (1999). *Am. Mineral.* **84**, 1902–1905.

Zhou, R.-S. & Snyder, R. L. (1991). *Acta Cryst.* B**47**, 617–630.